NASA

Technical Memorandum 82161

ELECTROMAGNETIC CASCADES IN PULSARS

J. K. Daugherty and Alice K. Harding

JULY 1981

National Aeronautics and Space Administration

Goddard Space Flight Center
Greenbelt, Maryland 20771

ELECTROMAGNETIC CASCADES IN PULSARS

J. K. Daugherty

Data General Corp.

and

Alice K. Harding

Laboratory for High Energy Astrophysics

NASA Goddard Space Flight Center

ABSTRACT

The development of pair-photon cascades initiated by high energy electrons above a pulsar polar cap is simulated numerically. The calculation uses the energy of the primary electron, the magnetic field strength, and the period of rotation as parameters and follows the curvature radiation emitted by the primary, the conversion of this radiation to e+ e- pairs in the intense fields and the quantized synchrotron radiation by the secondary pairs. A recursive technique allows the tracing of an indefinite number of generations using a Monte Carlo method. Gamma ray and pair spectra are calculated for cascades in different parts of the polar cap and with different acceleration models. We find that synchrotron radiation from secondary pairs makes an important contribution to the gamma ray spectrum above 25 MeV, and that the final gamma ray and pair spectra are insensitive to the height of the accelerating region, as long as the acceleration of the primary electrons is not limited by radiation reaction.

I. INTRODUCTION

Pulsar magnetospheres are believed to be extremely favorable environments for particle-photon cascades. Strong magnetic ($\gtrsim 10^{12}$ gauss) and electric ($\sim 10^{9}$ esu) fields near neutron stars can provide all of the necessary ingredients for these cascades: high energy particles, efficient radiation processes, and a pair production mechanism. In the present picture, particles are accelerated by rotation-induced electric fields above the polar cap and move along curved magnetic field lines. If the resulting curvature radiation from these particles extends to gamma ray energies $\sim$ 1 GeV, then the curvature photons have a high probability of producing electron-positron pairs in the magnetic and electric fields. The pairs resulting from magnetic pair production will in general be created with momentum components perpendicular to the field. Each member of the pair will therefore radiate synchrotron photons, many of which will be able to produce a second generation of pairs. This process will continue until the synchrotron photons are no longer energetic enough to pair produce. The surviving photons then constitute the observable high energy radiation from the pulsar, and the pairs may be input to a coherent process which produces the radio (and possibly optical) emission.

The importance of such cascades in accounting for the observed radiation from pulsars was originally pointed out by Sturrock(1971). Most current pulsar theories rely on electromagnetic showers for the production of the low energy particles which radiate coherently at radio wavelengths (Ruderman and Sutherland 1975,Cheng and Ruderman 1977, Arons and

Scharlemann 1979). Although these models differ as to how the accelerating electric fields are induced above the poles of the star, they all agree that pair production cascades will limit the potential drop below its maximum possible value.

Most of the models which have been proposed to explain gamma ray emission from pulsars focus on the curvature radiation from the accelerated primary particles and the attenuation in the magnetosphere due to pair production. Hardee (1977) showed that particles accelerated by the polar gaps proposed by Ruderman and Sutherland(1975) (hereafter referred to as RS) were capable of producing curvature gamma rays with energies in excess of 1 GeV. A detailed numerical model involving primary curvature radiation and pair production in the magnetosphere has since produced calculated gamma ray spectra which give good fits to the observed spectra of the Crab and Vela pulsars (Harding, Tademaru and Esposito 1978; Harding 1981). These calculations ignored the details of the acceleration mechanism and the radiation produced while the primaries were being accelerated. But analytical calculations of the spectrum produced by particles in the accelerating region (Ayasli and Ogelman 1980, Ayasli 1981) have shown that radiation reaction during the acceleration cannot be important in fast pulsars like the Crab and Vela, or the spectrum would be much flatter than observed. Therefore, the gamma radiation from the acceleration region should not be an important contribution to the total spectrum. It seems that, as a first approximation, the observed gamma ray spectra of the Crab and Vela pulsars are best explained as curvature radiation from high energy primaries which are losing energy (ie. are above the acceleration region). A calculation by Salvati and Massaro (1978), which made an attempt to include synchrotron radiation from the first generation of pairs suggested

that synchrotron gamma rays may also make an important contribution to the spectrum at energies below 1 GeV.

In this paper, we present a scheme for numerically simulating the cascade produced by a primary electron, which we have used to calculate the resulting gamma ray and pair spectra. The technique allows a comparatively accurate treatment of geometrical aspects of the cascade process, to which the resulting spectra are extremely sensitive. The calculation follows the curvature radiation emitted by the primary, the conversion of this radiation to electron-positron pairs, and the subsequent quantized synchrotron radiation by the secondary pairs. A recursive procedure is able to trace an indefinite number of higher generations of pairs produced by the synchrotron gamma rays. We investigate the contribution of radiation from all generations of pairs to the gamma ray spectrum above 25 MeV, the number of pairs produced per primary electron, and the energy distribution of the pairs. Details of cascade development in the acceleration region and the angular distribution of pairs and gamma rays from the cascade will be treated in another paper.

II. Numerical Simulation of Pulsar Cascades

In the model considered here, the magnetic field is assumed to be purely dipolar above the stellar surface. Electrons are drawn from stellar surface layers at the polar cap zones, and accelerated along the magnetic field lines up to a height comparable to the polar cap radius. Above this height, the magnetospheric plasma is assumed to cut off further acceleration, and the electric fields induced by the co-rotating plasma have no significant parallel component.

The calculation described here traces the cascade initiated by a single primary electron which originates from a given point on the polar cap. Its input parameters include the pulsar period and radius, the surface field strength and orientation of the magnetic field relative to the rotational axis, and the peak energy achieved through acceleration. Two versions of the calculation have been developed in order to treat both intantaneous and continuous acceleration.

A full cascade resulting from large numbers of primary electrons, whose energetic and spatial distributions over the polar cap zones are supplied as additional input parameters, can in principle be found by taking weighted results from separate single particle calculations of the type discussed here. Unfortunately, while the solutions found by Deutsch (1955) for the surface field configurations of magnetic stars in vacuo might suggest approximate forms for these distributions, the surface charge structure in pulsars surrounded by magnetospheres is not well known. The spectral results reported in Section III below are thus restricted to the case of primary acceleration from the outer rim of the polar cap. However, it will be shown that this case may be a good approximation to the actual time integrated spectrum from the polar cap.

The calculation involves two different reference frames: the rotating frame where the star and dipole field are stationary, and the nonrotating or observer's frame. Tracing of particle trajectories takes place in the rotating frame because they follow field lines, while tracing of photons takes place in the nonrotating frame where they follow straight line trajectories.

a) Primary electron trajectory

In the first version of the calculation, the energy of the primary electron at a given height above the stellar surface is specified as input. Above this height, the electron is assumed to "coast" outward along the field line corresponding to the chosen surface coordinates, losing energy via curvature radiation. The second version, which considers a continuous acceleration of the primary electron up to a height comparable to the polar gap heights suggested by RS, has also been studied. It turns out that as long as the acceleration region does not extend much further above the polar caps, the final gamma ray spectra which result from primary electrons with similar peak energies is not very different in the two versions (see Section III).

In both versions of the calculation, the outward trajectory of the primary electron is divided into segments of arc length Δs, over each of which the electron loses (at most) a fixed fraction $\eta = dE / E$ of its present energy, $E = \gamma mc^2$, due to curvature radiation. If the path length over which this fractional energy loss occurs should become large compared to dimensions over which the fields change, the segment length is limited to a fixed maximum value Δs_{max}, measured in units of the stellar radius R_c. In the version which includes acceleration of the primary electron, Δs_{max} must be further limited to an appropriate fraction of the acceleration height. The value $\eta = 0.1$ has been found sufficiently small to be adopted as a standard value in the calculations reported here. Values adopted for Δs_{max} are listed in Table 1(a).

The division into path segments is made by finding the exact radius of curvature,

$$\rho_c = \frac{K \sin\theta \, (1 + 3\cos^2\theta)^{3/2}}{3\,(1 + \cos^2\theta)} \qquad (1)$$

for the dipole field line, $r = K \sin^2\theta$, at the electron position (the starting point of the segment), and then estimating the total energy loss rate,

$$\left(\frac{d\gamma}{dt}\right)_{curv} = \frac{2}{3}\left(\frac{r_e}{\rho_c}\right)^2 \gamma^4 \qquad (2)$$

due to curvature radiation at that point (see for example Jackson 1975), where $r_e = e^2/m c^2$ is the classical electron radius. From this rate, the increment of arc length over which $(d\gamma/dt)(\Delta s/c) = \eta$ is derived. (If the calculated increment Δs is larger than the maximum value Δs_{max}, this maximum becomes the increment and the specified energy loss is replaced by the smaller loss over this increment.)

The energy loss from curvature radiation is subtracted and the gain due to acceleration, if any, is added to the energy at the start of the segment, so that the net energy change is

$$\Delta E = -mc^2 \left(\frac{d\gamma}{dt}\right)_{curv} \frac{\Delta s}{c} + e E_{\parallel} \Delta s \,. \qquad (3)$$

$E_{\parallel}$ is the electric field, parallel to the magnetic field, which accelerates the electron. We assume the simplest model where $E_{\parallel}$ is constant,

$$E_{\parallel} = \begin{cases} \frac{V}{h} & s \leq h \\ 0 & s > h \end{cases} \qquad (4)$$

where V is the potential drop and h is the extent of the acceleration region above the stellar surface. In the first version we consider, $V = 0$ (so that $E_{\parallel} = 0$ everywhere) and the electron trajectory starts at the stellar surface with initial energy E_0 equal to the maximum energy. In the second version, values are adopted for V and h, and the electron starts at the stellar surface with $E_0 = m c^2$ (ie. at rest), where it accelerates from $s = 0$ to $s = h$ along its magnetic field line. If the first term remains small compared to the second term in equation (3), then the acceleration will not be radiation reaction limited (NRR case) and the electron's maximum energy will be $E_3 = V$. If, however, the first term becomes comparable to the second term, the acceleration is radiation reaction limited (RR case), and the electron will achieve a maximum steady state energy,

$$\gamma_{..} = \left(\frac{V}{h \cdot m c^2} \quad \frac{e^2}{r_e^2} \quad \frac{3}{2} \right)^{1/4} ,$$

less than V, in a distance,

$$s_{ss} = \left(\frac{3}{2}\frac{E_c}{I_c}\right)^{1/4}\left(\frac{hmc^2}{V}\right)^{3/4}.$$

After equation (3) is used to find the new energy, the position is shifted along the dipole field line by the distance Δs. For this purpose, a table relating arc length displacements from the stellar surface to coordinates (r, θ) along the chosen field line is established at the beginning of the calculation.

b) Curvature radiation

Before the calculation proceeds to the next segment, the outward propagation of the curvature radiation emitted over the present segment, and the ensuing shower of secondary photons and electrons which it generates, are completely traced. This task is accomplished by a recursive procedure, whose inputs are the energy, initial position and time coordinates, and the direction cosines of a photon emitted at any given stage in the cascade development. Figure 1 schematically illustrates the cascade produced by a curvature radiation photon emitted during the first step in a primary electron trajectory.

At its lowest level, the procedure follows the "bundle" of curvature photons emitted from each segment. Since the segments over which most of the curvature radiation is emitted are quite short compared to characteristic lengths such as R_0 or the radius of the polar cap, the calculation assumes that all photons are emitted from the midpoint of the segment. Furthermore, the direction of emission (in the rotating frame of

the magnetosphere) for the entire spectrum of photons is taken to be that of the tangent to the field line at this point (since $\Delta\theta \sim 1/\gamma \ll 1$). In the non-rotating frame, where the calculation follows the photon to its pair conversion point, there is an aberration of the emission direction so that the photon will not initially be propagating tangent to the magnetic field in that frame.

The spectrum of curvature radiation may be found from classical electrodynamics (it is in fact identical to that of classical synchrotron radiation from an electron with the same radius of curvature) and may be written in the form (Jackson 1975),

$$\frac{dI_\omega}{d\omega} = \sqrt{3}\,\frac{e^2}{c}\,\gamma\,K\left(2\,\frac{\omega}{\omega_c}\right) \qquad (5)$$

where,

$$\omega_c = \frac{3}{2}\,\frac{c}{\rho}\,\gamma^3$$

is the cutoff frequency, and the function $K(x)$ is defined as,

$$K(x) \equiv 2x \int_{2x}^{\infty} K_{5/3}(x')\,dx' \qquad (6a)$$

It has the asymptotic forms:

$$K(x) = \begin{cases} 2.149\,(x^{1/3}) & x \ll 1 \\ 1.253\,x^{1/2}\,e^{-x} & x \gg 1 \end{cases} \qquad (6b)$$

which we use to evaluate the function in these limits. Around x = 1, the function values are interpolated from a table of calculated values. This spectrum is divided into increments $\Delta\omega$, and the "number" of photons Δn_{cr} in each spectral increment is estimated by dividing the energy, $(dI/d\omega)\Delta\omega$, contained within the increment by the average photon energy of that increment. The Δn_{cr} photons are all assumed to have this average energy. Standard values for the spectral parameters chosen in this calculation are given in Table 1(b).

The calculation in effect takes only one of the Δn_{cr} photons in each spectral increment and traces the cascade which that photon produces. Pair conversion is assumed to occur when its probability of survival, $P(x) = \exp[-\int(dx/\lambda)]$, after propagating a distance x through the ambient fields, has dropped to 1/e. Here, λ is the local mean free path for pair production. However, it is assumed that the cascades resulting from the other photons emitted within this same spectral increment at the same point are identical. That is, the secondary photon and electron spectra resulting from the one sample photon are multiplied by Δn_{cr} before adding their contribution to the accumulated gamma ray spectrum.

This use of the relative numbers of photons in each increment as a weighting factor is done only for the curvature radiation photons, since the synchrotron radiation emitted subsequently by secondary electrons is both quantized and random in azimuthal direction, and requires the tracing

of individual photons. The assumption that pair production occurs when when $P(x)=1/e$ is therefore made only for the curvature photons. Pair production points for the synchrotron photons are determined by giving them each a random probability of survival. A pure Monte Carlo approach would also require the tracing of curvature photons on an individual basis, but this averaging approximation has been adopted to avoid prohibitive time requirements. The principal justification for this approach lies in the fact that the mean free paths for the energetic curvature photons are typically short compared to the stellar dimensions, so that the dispersion in these distances may be neglected in tracing the cascade development. In addition, it may be noted that the final cascades produced by curvature photons are typically quite large, and hence those cascades initiated by parent photons which are identical in energy, position, and direction should be statistically similar.

c) Pair production

We have investigated several methods for following the outward propagation of the photons through the magnetosphere. This procedure is quite sensitive to the choice of path-length increments, since the attenuation coefficient for magnetic pair production is a strongly varying function of the strength and orientation of both the magnetic and electric fields. In addition, the photon follows essentially a straight-line trajectory in the nonrotating frame (ignoring general relativistic effects and slight deviations due to refractive properties of the intense field), while the star and the near-zone fields rotate beneath it. As mentioned earlier, the aberration of the emission direction must also be taken into account. The inclusion of photon aberration is crucial in correctly determining the initial pair production rate (Harding et. al. 1978). All of these effects must be treated carefully in order to arrive at reasonably

accurate pair conversion points. Of the methods explored to date, the most satisfactory approach has been to use initially small increments in the photon path lengths, which are dynamically rescaled to greater (and less time consuming) values as permitted by the step-by-step changes in the ambient fields. The parameters adopted in this procedure are shown in Table 1(c).

The expressions used here for the pair production attenuation coefficients are those found by Daugherty and Lerche (1975), which include the modifications to the attenuation coefficients in pure magnetic fields (Toll 1952; Erber 1966; Tsai and Erber 1974) due to the presence of perpendicular electric fields (where $B^2 - E^2 > 0$ and $\underset{\sim}{E}\cdot\underset{\sim}{B} = 0$). Without loss of generality, a frame may be chosen such that $\underset{\sim}{B} = B\,\hat{z}$ and $\underset{\sim}{E} = E\,\hat{y}$, in which case the (unpolarized) attenuation coefficient for a photon with arbitrary direction cosines (η_x, η_y, η_z) has the asymptotic form,

$$\zeta(\omega, E, B) = 0.23 \frac{\alpha}{\lambda_c} \frac{B}{B_{cr}} \left[\left(\eta_x - \frac{E}{B}\right)^2 + \eta_y^2\left(1 - \frac{E^2}{B^2}\right)\right]^{1/2}$$

$$\exp\left\{-\frac{2}{3}\frac{m}{\omega}\left[\left(\eta_x - \frac{E}{B}\right)^2 + \eta_y^2\left(1 - \frac{E^2}{B^2}\right)\right]^{1/2}\right\} \qquad (7)$$

in the limits $B/B_{cr} \ll 1$, $E_\gamma/mc^2 \gg 1$, where $B_{cr} = m^2c^3/e\hbar$ is the critical field strength.

Although the surface acceleration model used here implies that the above condition $\underset{\sim}{E}\cdot\underset{\sim}{B} = 0$ is not satisfied everywhere, the validity of equation (7)

is not significantly affected even when $E \cdot B$ does not vanish. In fact, the effects of parallel components of electric fields have been found to be negligible for the photon optical depths (Harding et. al. 1978; Ayasli 1978), even for the upper limits based on the vacuum model (Deutsch 1955).

At the conversion point, both members of the pair are assigned the same direction and half the energy of the parent photon. These high energy approximations are reasonable (Ayasli 1978) for the cascade model, but have been made here for the equally cogent reason that no detailed investigation of the angular and spatial distributions in magnetic pair production is known to us. If the present calculation should be extended to moderate or low energy gamma ray emission, such information would probably be required to derive accurate spectra.

d) Quantized synchrotron radiation

The initial pair direction is used to estimate the initial particle energy tranverse to the local magnetic field. In general, this energy will be considerably higher than the local (quantized) ground state energy, and each member of the pair must rapidly lose this energy through a burst of quantized synchrotron radiation. It is important to note that, in contrast to curvature radiation, the photon energies from synchrotron radiation in superstrong magnetic fields are typically comparable to the energies of the particles themselves. Moreover, the emission rates are so rapid (even after the Lorentz time-dilation effects due to parallel motion are taken into account) that essentially all the initial tranverse energies of the created pair are lost before the particles can move a significant distance outward along the local field line. For both of these reasons, the

contribution of the synchrotron component to the emergent gamma ray spectrum has been found to be quite significant. (In contrast, the curvature radiation from all generations of the secondary electrons has been estimated to make a negligible contribution to the final spectra, at least above 25 MeV. For $B \lesssim 8 \times 10^{12}$ gauss, synchrotron radiation from the pairs always dominates, because $\gamma \sin\psi > 1$ for the photons which pair produce.) An additional consequence of the rapid emission rates is that acceleration of the pairs during their synchrotron burst will be negligible.

In order to follow each member of the pair through its synchrotron emission sequence, the equation of the dipole field line which passes through the conversion point is found and the particle momentum parallel to the field line is inferred from its initial angle to the field, ψ. This parallel momentum in fact determines a "longitudinal" Lorentz factor

$$\gamma_{\parallel} = \left(\sin^2\psi + \frac{1}{\gamma^2}\cos^2\psi \right)^{-1/2}$$

which is a conserved quantity under the approximations adopted here.[1] For each member of the pair in turn, the calculation then follows the quantized synchrotron emission sequence as the electron drops toward its ground state orbital in the local field. For each photon emission, a series of Lorentz transformations are made to orient the coordinate axes along the field line

[1] This calculation has assumed that the synchrotron photons are all emitted in the orbital plane of the electron, in the frame where the electron moves transverse to the B field. In this approximation, $\gamma_{\parallel}$ is strictly conserved since the recoil of the electron when it emits a photon cannot change its energy parallel to the field. We have verified numerically that $\gamma_{\parallel}$ is conserved in this case.

and remove the longitudinal motion, emit a photon in the frame of purely "circular" motion, and then return the energy and direction of the emitted photon in the original (stellar) frame. The quantized emission spectrum given by Erber (1966),

$$I(E,\omega,\Gamma) = \frac{\sqrt{3}\,\alpha}{2\pi}\,\frac{mc^2}{\lambda_c}\left(\frac{\Gamma}{E}\right)\left(1-\frac{\hbar\omega}{E}\right)K(2S)$$

where, $\Gamma = \left(\frac{E}{mc^2}\right)\left(\frac{\Gamma_0}{\Gamma_{cr}}\right)$, $S = \frac{y}{2+3\Gamma(1-y)}$,

$$y = \frac{\omega}{\omega_{cr}}, \qquad \omega_{cr} = E\,\frac{3\Gamma}{2+3\Gamma} \qquad (5)$$

has been used to sample the photon energies in the transverse frame. The $K(x)$ function [cf. eqn. (6)] is the same as that appearing in the curvature radiation spectrum. The photons are assumed to be emitted in the plane of the electron orbit with random azimuthal angles.

The recursive aspect of the calculation appears at this point, since for each emitted synchrotron photon the entire procedure of tracing the photon propagation to its annihilation point (or until it has been determined to have escaped conversion), followed by the tracing of its resultant pairs through the synchrotron emission sequence, is begun anew. The recursion may be pushed to an indefinite number of levels, depending on the number of successive photon and pair generations emerging in the cascade. The process is eventually brought to a conclusion when the lower energy photons belonging to the succeeding generations escape from the magnetosphere without pair producing. In addition to the energy degradation, the rapid decrease in field strengths with distance from the star is also instrumental in ending the cascade. Table 2 indicates typical levels of recursion (generation numbers) encountered in calculations with varying

surface field strengths and primary electron energies.

After the calculation finishes tracing the complete shower due to the emission of a given synchrotron photon, the transverse energy of the electron which produced that photon is reduced by the amount of the emitted photon energy, and the electron is displaced outward along its guiding field line by a distance estimated from the total synchrotron emission rate,

$$\frac{\Delta E}{\Delta x} = \frac{2}{3} \lambda \frac{[illegible]^2}{\lambda_c} G(\Gamma) \qquad (1)$$

Here, $G(\Gamma)$ is the loss rate function defined by Erber (1966).

The synchrotron emission process is then repeated for this electron until its energy drops below a suitable threshold, taken here to be 100 MeV. When this process has been completed for each member of the pair in turn, the procedure returns to the next lower level of recursion. At the lowest level, namely that of the primary electron, the electron is displaced along its outward trajectory as described above, and the next bundle of curvature photons is traced.

The calculation accumulates a spectral distribution of all gamma rays above a certain cutoff energy (here taken to be 25 MeV) which are found to escape pair conversion in the magnetosphere. Spectral distributions are also obtained for the accumulated generations of pairs, in which the "final" energy of each electron or positron is taken to be its energy parallel to the magnetic field, $\gamma_{//}$, which is conserved. The final energy of pairs produced in the accelerating region is,

$$E_1 = \gamma_{11} mc^2 \pm \sqrt{(\gamma_{11}-s)/\gamma_1} \qquad (14)$$

so that electrons (+sign) are accelerated away from the star and positrons (-sign) are accelerated back towards the stellar surface. This gain or loss of pair energy parallel to the field will not affect the sychrotron radiation, because of the short radiation timescales, but if a member of the pair should gain enough energy, its curvature radiation may contribute to the final spectrum. We do not consider this contribution in the present version of the calculation. These spectra are found mainly as a check on the overall energy distributions among particles in the final cascade. No attempt has been made here to trace their subsequent (and much lower) losses due to curvature radiation, nor to guess at any subsequent acceleration these particles may undergo as they approach the light cylinder. In addition to the spectral distributions, the multiplicity, $M = (N_s^+ + N_s^-)/N_p$, or the ratio of secondary to primary particles, is also found.

III. RESULTS

a) Gamma-ray spectra

The first version of the calculation, as described in Section II, ignores the details of the acceleration and assumes that the primary electron is instantaneously accelerated to energy E_o at the stellar surface. As we will show later in this section, acceleration over a finite distance for parameters of current polar cap models does not change the calculated spectrum significantly. Figure 2 shows the build-up of the primary curvature spectrum and the accumulation of escaping photons from the

cascade as the primary electron steps out along its trajectory. The curvature spectrum for the first few steps has the characteristic -2/3 slope but, as the primary loses energy, the shift of the curvature cutoff to lower energies steepens the spectrum to an asymptotic slope of -5/3. Because the radius of curvature of the field line also increases as the electron moves outward, the contribution to the final curvature radiation spectrum from successive steps decreases. We find that for the parameters listed in Table 1, the contributions become negligibly small above the 20th step. The cascade gamma ray spectra from the first 3 steps have extremely sharp high energy cutoffs, indicating that virtually all photons above 500 MeV (and many below 500 MeV) are efficiently converted to pairs and lower energy photons. In fact, in these first few steps near the stellar surface, the gamma ray spectrum is almost entirely dominated by synchrotron photons. Curvature radiation from higher steps farther away from the star, where the fields have decreased and photons can escape more easily, fills in the high energy part of the final spectrum. The final high energy cutoff is a balance between the decreasing optical depth of the magnetosphere (the increasing energy of the escaping photons) and the decreasing cutoff energy of the curvature radiation along the trajectory.

The calculation shown in Figure 2 followed the cascade initiated by an electron moving on the outermost open field line (ie. at the edge of the polar cap). Figure 3 shows the final gamma ray spectrum from 10^{13} eV electrons on field lines originating at different magnetic colatitudes, θ_c, on the stellar surface [in units of the polar cap half angle defined by $\sin\theta_c = (R_c/c)^{1/2}$]. There are basically two effects which change the spectrum as a function of θ_c, and they are both due to the magnetic field line radius of curvature. First, the increase in radius of curvature

toward the magnetic pole gives a lower curvature radiation cutoff, so there are fewer high energy photons to feed the cascade. Second, the larger radius of curvature lowers the pair production optical depths, since photons will have to travel further to encounter a sizable perpendicular field component. This allows higher energy photons to escape, decreasing the synchrotron contribution to the final spectrum. Clearly, the most extensive cascades are produced by electrons accelerated near the edge of the polar cap. The observed time integrated spectrum from the pulsar would be an average of the spectra produced by electrons at different θ_c across the pulse, weighted by the primary flux across the polar cap. The case $\theta_c = \theta_{c_-}$ is probably the best approximation to the time-integrated spectrum since i) most of the gamma ray flux is produced in cascades from primaries with $\theta_c = \theta_{c_-}$ ii) most of the area swept out by random observer lines of sight to a pulsar will be in the outer parts of the polar cap iii) in current models, acceleration is strongest at the edges of the polar cap iv) the variation of the spectral index with θ_c is small except near the poles.

The dependence of the calculated gamma ray spectrum on pulsar period is shown in Figure 4. The steepening of the spectrum with decreasing period results primarily from the increasing magnetic colatitude of the outermost open field line (cf. Fig. 3) Also important for short periods is the increase in the pair production optical depths due to the rotation-induced electric field. Because of these effects and the arguments given in the preceding paragraph, short period pulsars should have steeper gamma ray spectra.

In the second version of the calculation, the primary electrons are accelerated to a specified energy over a finite distance above the polar cap. The contribution to the gamma ray spectrum from this accelerating region is shown in Figure 5 for different values of the voltage and the acceleration distance. Cases A1 and A2 have parameter values which are approximately those estimated by RS and Arons and Scharlemann (1979) respectively for the Crab pulsar. In each of these cases the accelerating particles do not experience strong radiation reaction (the second term in Eqn. [3] dominates) and they gain an energy E_3 equal to the potential drop V. Case A3 is radiation reaction limited (the first term becomes equal to the second in Eqn. [3]) and the electron reaches its steady state energy, about 10^{13} eV after traversing only half of the accelerating region. The gamma ray flux from acceleration regions A1 and A2 is negligible at all energies compared to the gamma ray flux produced above the acceleration region. This is because, for values of h less than or comparable to the polar cap radius, the distance traveled during acceleration is much smaller than the typical length scale over which the particle loses its energy from curvature radiation. Furthermore, when the acceleration is not radiation reaction limited, the particle travels a relatively short distance near its maximum energy while it is being accelerated. For larger acceleration heights as in case A3, the electron spends more time at or near its maximum (steady state) energy and therefore, the contribution to the gamma ray spectrum is greater. However, acceleration heights this large at the polar cap will be unstable against pair production breakdown (RS). In fact, in case A3 we find pairs produced well within the region $s < h$. Polar acceleration regions will generally be non-radiation reaction limited, except possibly in long period pulsars. The pairs and gamma rays produced in the acclerating region are therefore not an important contribution to

the final gamma ray or pair spectra. However, they are undoubtedly important in determining the structure and dynamics of the accelerating region, and we hope to consider this problem in future work.

Figures 6a and 6b show gamma ray spectra for periods of the Crab and Vela pulsars, each calculated for three different values of the surface magnetic field strength. In these calculations, the electron is started from the stellar surface with $E_0 = 10^{13}$ eV and does not experience any further acceleration along its trajectory. The effect of increasing the magnetic field is to steepen the spectrum by producing a more extensive cascade. A higher field increases the pair production optical depths, removing high energy photons from the primary spectrum and converting them, through synchrotron radiation, to low energy photons. A shorter period amplifies this effect, as discussed previously, through higher pair production and decreased radii of curvature of the field. The observed COS-B data points for the Crab and Vela seem to best fit the $B_\perp = 10^{12}$ gauss spectra for both pulsars.

b) Pair spectra

The calculation also keeps track of the total number of pairs produced in a cascade as well as the number of pairs in each energy bin. Figure 7 shows the differential number spectrum of secondary electrons and positrons from a cascade having parameters of the Crab pulsar. These energies are the computed energy components of each member of the pair parallel to the magnetic field at the time they are produced. Changes in the spectrum due to Compton scattering or annihilation may occur, but the present calculation does not include such effects. Subsequent radiation losses,

however, should be negligible unless the particles are accelerated. The spectrum is roughly a power law with a cutoff at around 5 GeV. This high energy cutoff moves up for stronger fields, because the highest energy photons produce pairs at smaller angles , giving the pairs larger parallel energies. The low energy turnover is a real effect and not a result of the photon energy cutoffs. It results rather from the geometry of the fields, which determine very critically the lowest energies of the pair-producing photons and the angle to the field at which the pair is produced. The pair spectra for cascades in stronger fields have lower turnover energies because lower energy photons are able to produce pairs.

Results for the multiplicity, or the total number of electrons and positrons produced per primary electron in the cascade, for values of magnetic field strength and period are shown in Figure 8. No pairs are produced for fields below 10^{10} gauss for the period of the Crab. Above this field strength, the number of pairs rises sharply and then begins levelling off around a field strength of 10^{12} gauss. The cascade multiplicities for the Vela period, P = .089 s, are lower by a factor of 2 or 3. Multiplicities also decrease as the magnetic colatitude of the primary electron decreases for reasons discussed in Section IIIa. For typical field strengths around 10^{12} gauss, multiplicities of 10^{3} are easily achieved. While these numbers are much smaller than those originally estimated for pulsar cascades by Sturrock (1971), they are in good agreement with those estimated by RS. The total energy in photons emerging from the cascade exceeds the total energy in pairs for fields below 5×10^{12} gauss, but above this field strength the energy in pairs exceeds the energy in photons. This suggests that short period pulsars with high field strengths may lose a greater fraction of their rotational energy in particles than in radiation.

It is possible to estimate the primary and secondary particle fluxes from the Crab and Vela pulsars from these results, using the observed gamma ray fluxes to normalize the computed gamma ray spectra at $B_{\perp} = 10^{12}$ gauss. The primary electron flux required to give the observed gamma ray flux levels is $6 \times 10^{33}\ s^{-1}$ for the Crab (assuming a distance of 2 kpc.) and $2 \times 10^{33}\ s^{-1}$ for Vela (assuming a distance of 0.5 kpc.). These fluxes are of the same order of magnitude as the flux of particles expected from breakdown of a polar gap, which is

$$\dot{N}_1 \simeq n_0 \pi r_1^2 c N_s = 1.4 \times 10^{33} B_{12} P^{-2} N_s$$

where N_s is the number of secondaries produced per primary in the gap which are accelerated to energies comparable to the primary, and $n_0 = 7 \times 10^{10} P^{-1} B_{12}\ cm^{-3}$ is the corotation charge density at the stellar surface. With the calculated multiplicities for a complete cascade, the secondary particle flux from the Crab would be $3 \times 10^{37}\ s^{-1}$ and the secondary particle flux from Vela would be $4 \times 10^{36}\ s^{-1}$. This particle flux from the Crab is almost 4 orders of magnitude less than the $10^{41}\ s^{-1}$ estimated by Sturrock (1971).

IV. DISCUSSION

This paper has developed a technique for tracing electromagnetic cascades near pulsar polar caps. We have presented results of numerical calculations which predict the gamma ray and pair spectra for a standard

polar cap model and have shown that the predicted gamma ray spectra for the Crab and Vela pulsars are in good agreement with the observed spectra. Furthermore, it has been shown that a polar gap origin for the observed gamma rays less than 5 GeV is energetically feasible. This conclusion differs from that of Ayasli and Ogelman (1980) who conclude that polar gaps or acceleration regions near the poles make a negligible contribution to the total gamma ray emission compared to the outer gaps which have been proposed by Cheng and Ruderman (1977). They argue that the number of pairs involved in each polar gap breakdown is a factor of 10^{2} P lower than the number of pairs from an outer gap breakdown. Since these pairs would produce much of the gamma ray emission around 100 MeV, the gamma ray emission from the polar gap would, in their model, be lower than that from the outer gap by the same factor. However, they neglect the contribution from secondary pairs produced by cascades from the accelerated primaries above the polar gap. From our results, this synchrotron contribution provides about a factor of 10 increase in conversion efficiency of primary electron energy to gamma rays in the Crab, which compensates for the lower particle flux from the polar gap.

We have found that the gamma rays produced while the primary electron is accelerating to its maximum energy make a negligible contribution to the final gamma ray spectrum for stable polar accelerating potentials. Higher potential drops or larger acceleration regions would make more substantial contributions, but would probably be unstable. Exactly where and how these accelerating potentials break down are problems which could be investigated in detail with the technique developed here. A particularly interesting question is whether the potential drops are limited by synchrotron - pair production cascades at the top of the acceleration

region, thus producing a quasi-steady discharge as suggested by Arons and Scharlemann (1979), or whether the curvature radiation - pair production cascades proposed by RS can completely short out the parallel electric field. In the first case, the voltage and particle fluxes are constant in time while in the second case, they are time variable. Which case actually occurs in pulsars is of central importance to radio emission theories, and it hinges on whether the secondary pairs can be accelerated to primary energies and radiate high energy curvature photons.

The presence of higher magnetic field multipoles has been suggested in pulsar models. These multipoles could affect the near field structure by decreasing the radius of curvature of field lines. This would cause an increase in both the energy of the curvature photons and in the pair production rates in cascades near the surface, possibly producing steeper spectra than we have calculated for pure dipoles, and certainly producing more extensive cascades.

The result that cascades at different magnetic colatitudes produce different gamma ray spectra suggests that there should be observable spectral variations across the gamma ray pulse. There is observational evidence for this in the Vela pulsar (Kanbach et. al. 1981), although it is not clear where the gamma ray pulses are originating because of their phase lags relative to the radio pulse. Detailed predictions of spectral variations with pulse phase would require a more complete model of cascade development across the polar cap. The variations found in the flux of gamma rays with magnetic colatitude also suggests that the possible observed flux variations in the Crab pulsar (Greison et. al. 1975; Wills 1980) could be due to neutron star precession, presenting different parts of the polar cap to the observer at different times.

The calculation described in this paper could be refined and extended, in particular to cover lower gamma ray energies and to investigate pulse shapes and temporal behavior. Those approximations which have been made to avoid long computation times may be refined without great difficulties. However, several of the approximations mentioned above have been necessary because the physical processes involved are not sufficiently well understood. In the case of synchrotron radiation in superstrong magnetic fields, convenient analytic forms for the fully quantum mechanical regime are not available. The expressions used in the present calculation are inaccurate when the energy of the emitted photon approaches the energy of the electron, a situation quite probable for field strengths in excess of 10^{12} gauss. The approximation that the energy of the electron parallel to the magnetic field is conserved may also be incorrect when radiation reaction effects are important (Shen 1979). In this case, the angular distribution of the emitted photons must be considered, so that the recoil of the electron parallel to the field may be taken into account. In the case of pair production, the energy and angular distribution of the pairs is not well known. The high energy approximations made in this calculation (that the pair share the energy of the photon equally and that they initially travel in the same direction as the parent photon) are good only for photon energies $E_\gamma >> m c^2$. These fundamental processes must be investigated in greater detail before the technique described here can be extended to lower gamma ray energies.

We would like to thank D. J. Thompson and S. Ayasli for discussions and helpful comments.

REFERENCES

Arons, J. and Scharlemann, E. T. 1979, Ap. J.,231,854.

Ayasli, S. 1978, Ph.D. Thesis, Middle East Technical University, Ankara, Turkey (unpublished).

Ayasli, S. 1981, Ap. J., in press.

Ayasli, S. and Ogelman, H. 1980, Ap. J.,237,227.

Cheng, A. and Ruderman, M. A. 1977, Ap. J.,214,598.

Daugherty, J. K. and Lerche, I. 1975, Ap. Space Sci., 38,437.

Deutsch, A. J. 1955, Annales D'Astrophysique,18,1.

Erber, T. 1966, Rev. Mod. Phys.,38,626.

Greisen, K., Ball, S. E., Campbell, M., Gilman, D., Strickman, M., McBreen, B. and Koch, D. 1975, Ap. J.,197,471.

Hardee, P. E. 1977, Ap. J.,216,873.

Harding, A. K. 1981, Ap. J., ,245,267.

Harding, A. K., Tademaru, E. and Esposito, L. W. 1978, Ap. J.,225,226.

Jackson, J. D. 1975, Classical Electrodynamics (2nd edition) (New York: Wiley & Sons).

Kanbach, G. et. al. 1981, Astron. Astrophys., in press.

Lichti, G. G. et. al. 1980, Non-Solar Gamma-Rays(COSPAR), ed. D. Wills and R. Cowsik, p.

Ruderman, M. A. and Sutherland, P. G. 1975, Ap. J.,196,51.

Salvati, M. and Massaro, E. 1978, Astron. Astrophys.,67,55.

Shen, C. S. 1979,Phys. Rev. Letters,24,410.

Sturrock, P. A. 1971, Ap. J.,164,529.

Toll, J. S. 1952, Ph.D. Thesis, Princeton University (unpublished).

Tsai, W. and Erber, T. 1974, Phys. Rev. D,10,492.

Wills, R. D. 1980, Royal Society Meeting, London.

TABLE 1

CASCADE PARAMETERS

a) Primary electron trajectory

Number of steps	20
Maximum fractional energy loss per step	0.1
Maximum step length (Δs_{MAX}) $s < h$: RR	$s_{RR}/5$
NRR	$h/5$
$s \geq h$	R_c

b) Curvature spectrum

High frequency cutoff ($2\omega_{MAX}/\omega_c$)	7.0
Low frequency cutoff ($2\omega_{MIN}/\omega_c$)	0
Spectral increments per decade	10
Absolute low energy cutoff	100 MeV

c) Pair production

Initial step length in photon path	1 cm
Factor by which steps increase	10
Low field cutoff (B / B_{cr})	10^{-4}

d) Synchrotron spectrum

High frequency cutoff	E_c
Low frequency cutoff	25 MeV
Spectral increments per decade	3

TABLE 2

CASCADE PHOTON GENERATIONS[a]

INITIAL PRIMARY ENERGY E_c (eV)	MAGNETIC FIELD STRENGTH B_o (GAUSS)			
	10^{11}	5×10^{11}	10^{12}	5×10^{12}
5×10^{12}	—	—	3	4
1×10^{13}	3	3	4	4
2×10^{13}	—	—	5	—
5×10^{13}	—	—	—	7

[a] For P = .033 s, $\theta_o = \theta_c$

FIGURE CAPTIONS

Figure 1 - Schematic representation of a pair photon cascade initiated by an accelerated electron above the polar cap of a pulsar. Four generations of photons, including both curvature radiation photons, γ_{CR}, and synchrotron radiation photons, γ_{SR}, are shown.

Figure 2 - Cumulative spectra of primary curvature radiation photons (dashed line) and cascade photons (solid line) for various steps in the primary electron trajectory.

Figure 3 - Final gamma-ray spectra from cascades initiated by 10^{13} eV electrons at different magnetic colatitudes, θ_c in units of the polar cap half-angle, for a surface field of 10^{12} gauss and period of .033 s.

Figure 4 - Final gamma-ray spectra for different pulsar periods all with initial electron energy 10^{13} eV, surface field 10^{12} gauss and magnetic colatitude $\theta_c = 1.0$

Figure 5 - Gamma-ray spectra from the accelerating phase of the primary electron trajectory compared

to the final gamma-ray spectrum produced in the case of instantaneous acceleration. Case A1 has $V = 10^{13}$ eV and $h = 10^{3}$ cm., case A2 has $V = 10^{15}$ eV and $h = 10^{4}$ cm., case A3 has $V = 2 \times 10^{15}$ eV and $h = 10^{5}$ cm, while case A0 corresponds to $V = 0$, $h = 0$, and $E_0 = 10^{13}$ eV.

Figure 6 - Gamma-ray spectra for the periods of the a) Crab and b) Vela pulsars and three different values of the surface field strength in units of 10^{12} gauss. Also plotted are observed spectra for each pulsar from Lichti et. al. (1980).

Figure 7 - Differential e+ e- spectrum from a cascade with initial electron energy 10^{15} eV, surface field 10^{12} gauss, magnetic colatitude $\vartheta_0 = 1.0$, and period of the Crab, P = .033 s.

Figure 8 - Cascade multiplicity versus surface field strength for the periods of the Crab and Vela pulsars and also for a more typical pulsar period of 0.5 s. All calculations have $E_0 = 10^{15}$ eV, and $\vartheta_0 = 1.0$.

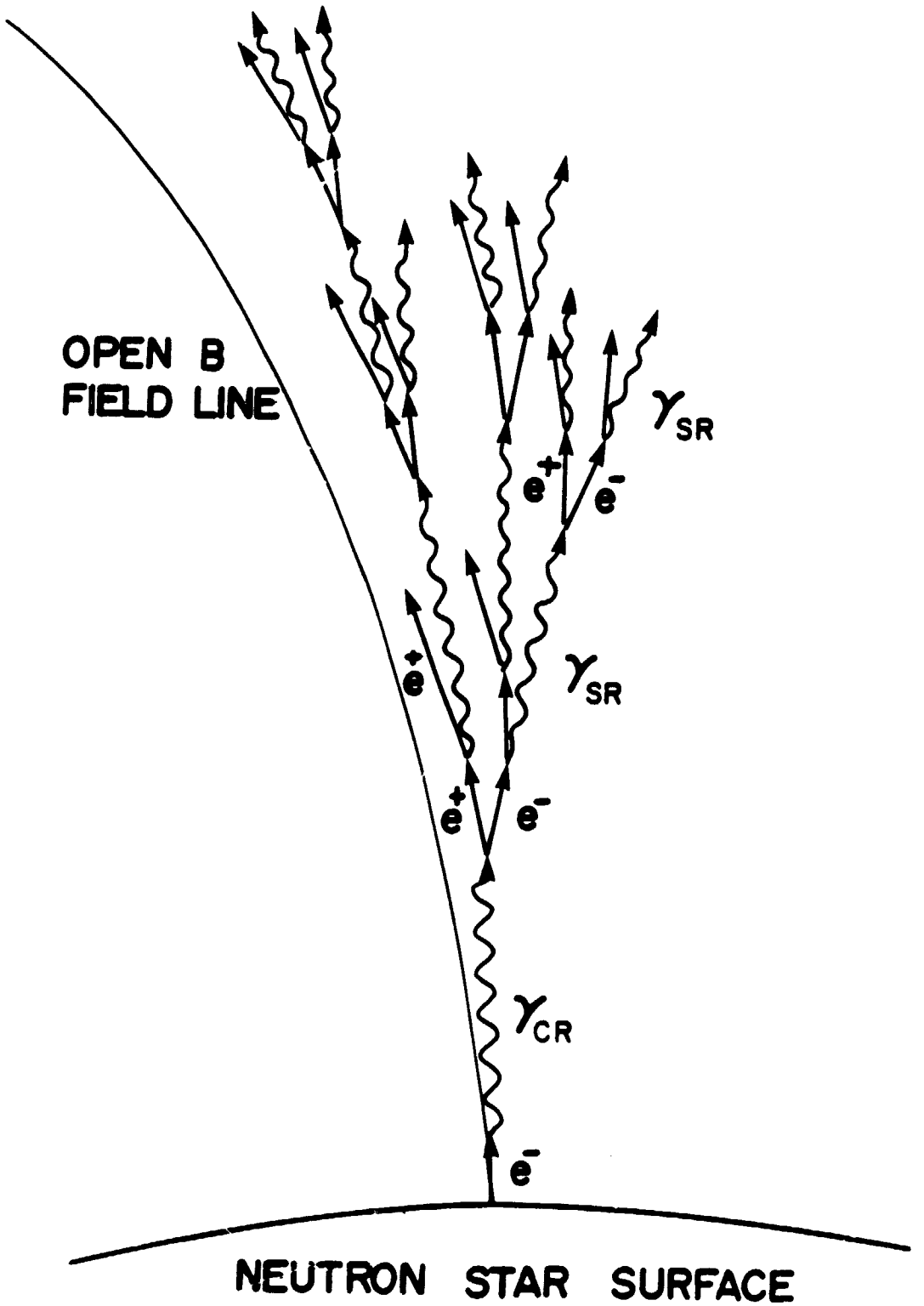
OPEN B
FIELD LINE
γ_{SR}
e^+
e^-
γ_{SR}
e^+
e^-
γ_{CR}
e^-
NEUTRON STAR SURFACE

Figure 1

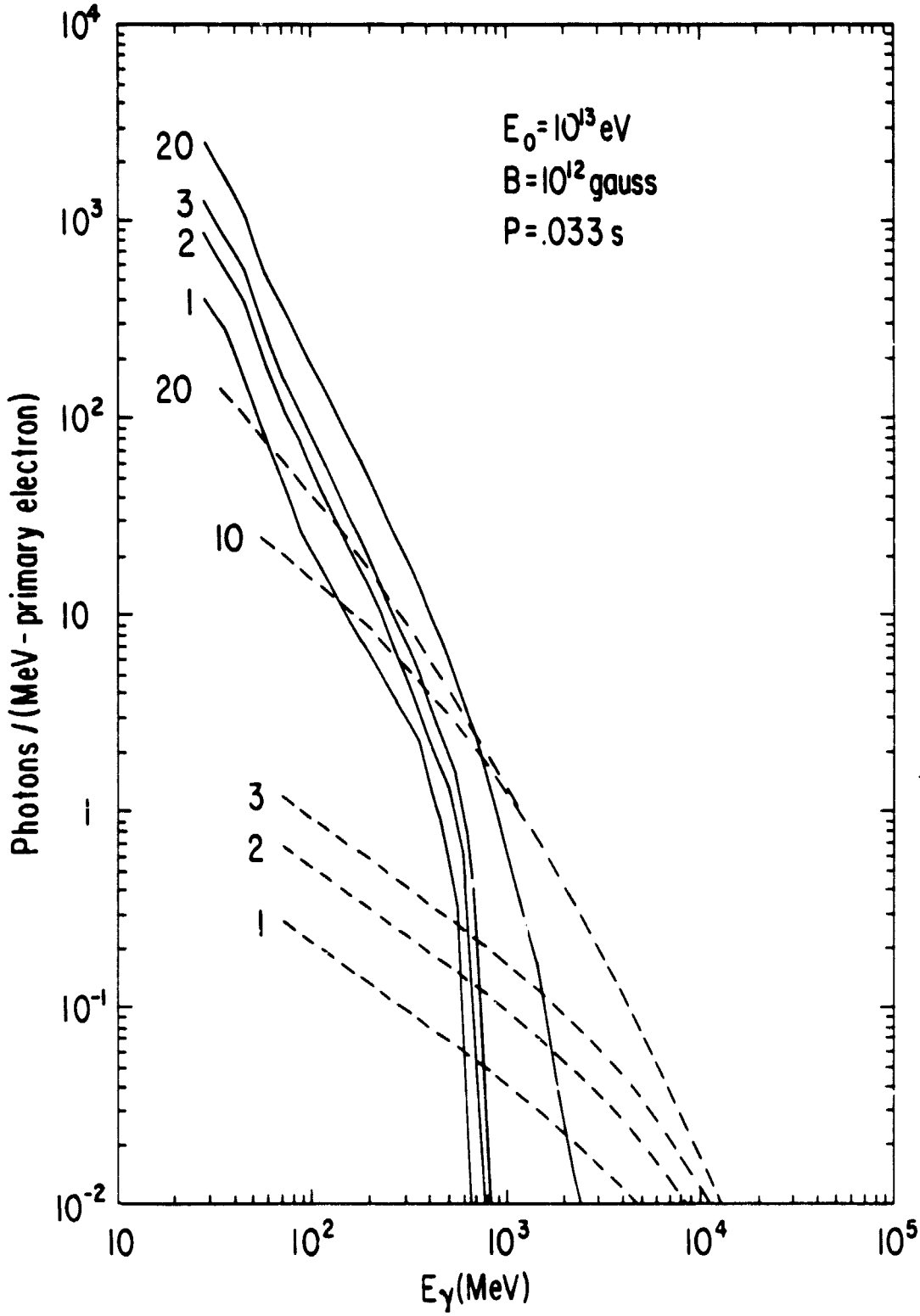
$E_0 = 10^{13}$ eV
$B = 10^{12}$ gauss
P = .033 s
20
3
2
1
20
10
3
2
1
Photons / (MeV - primary electron)
E_γ (MeV)
10^4
10^3
10^2
10
1
10^{-1}
10^{-2}
10
10^2
10^3
10^4
10^5

Figure 2

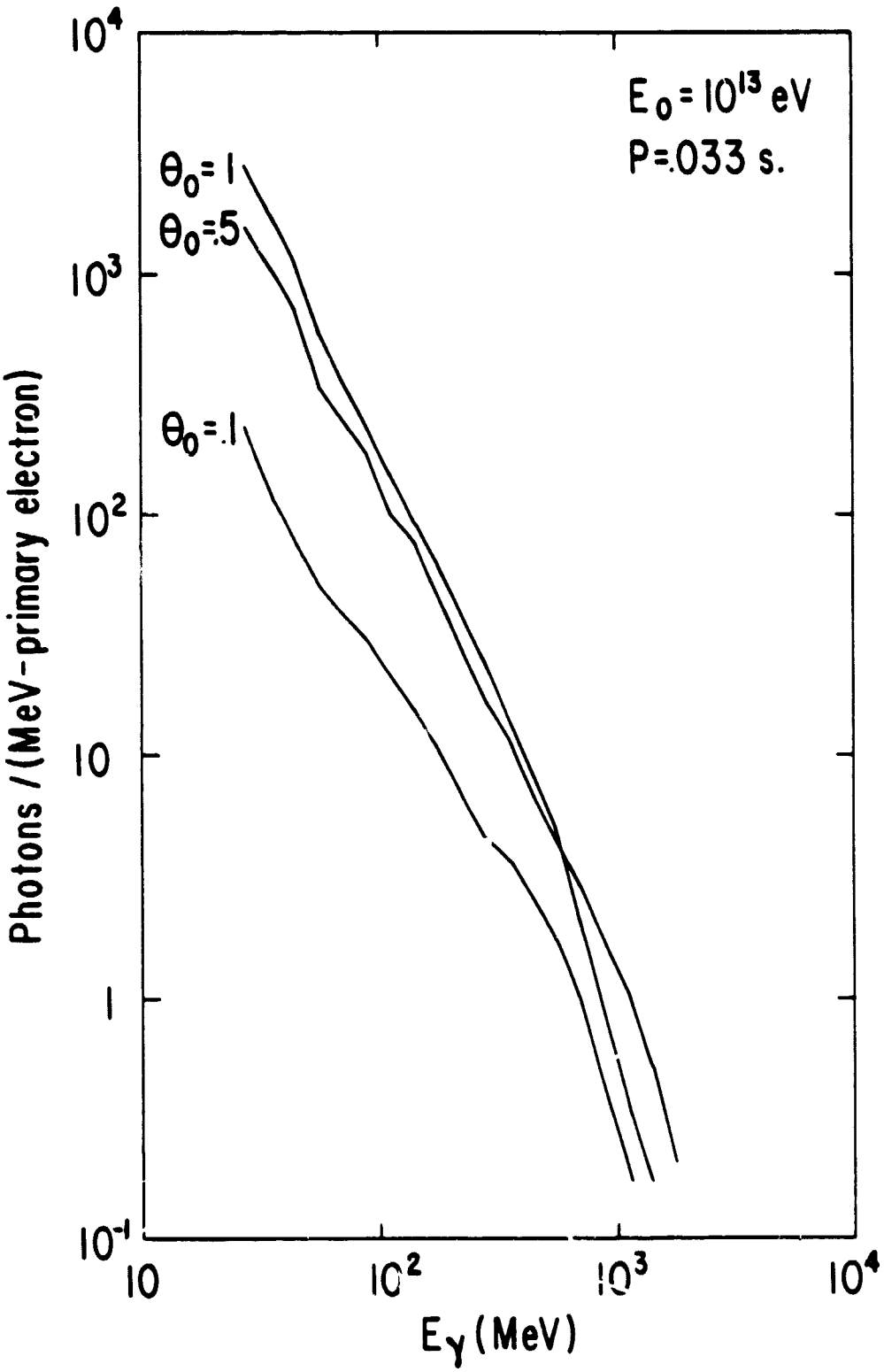
10^4
10^3
10^2
10
1
10^{-1}
$E_0 = 10^{13}$ eV
P=.033 s.
θ_0=1
θ_0=5
θ_0=.1
Photons /(MeV-primary electron)
10
10^2
10^3
10^4
E_γ (MeV)

Figure 3

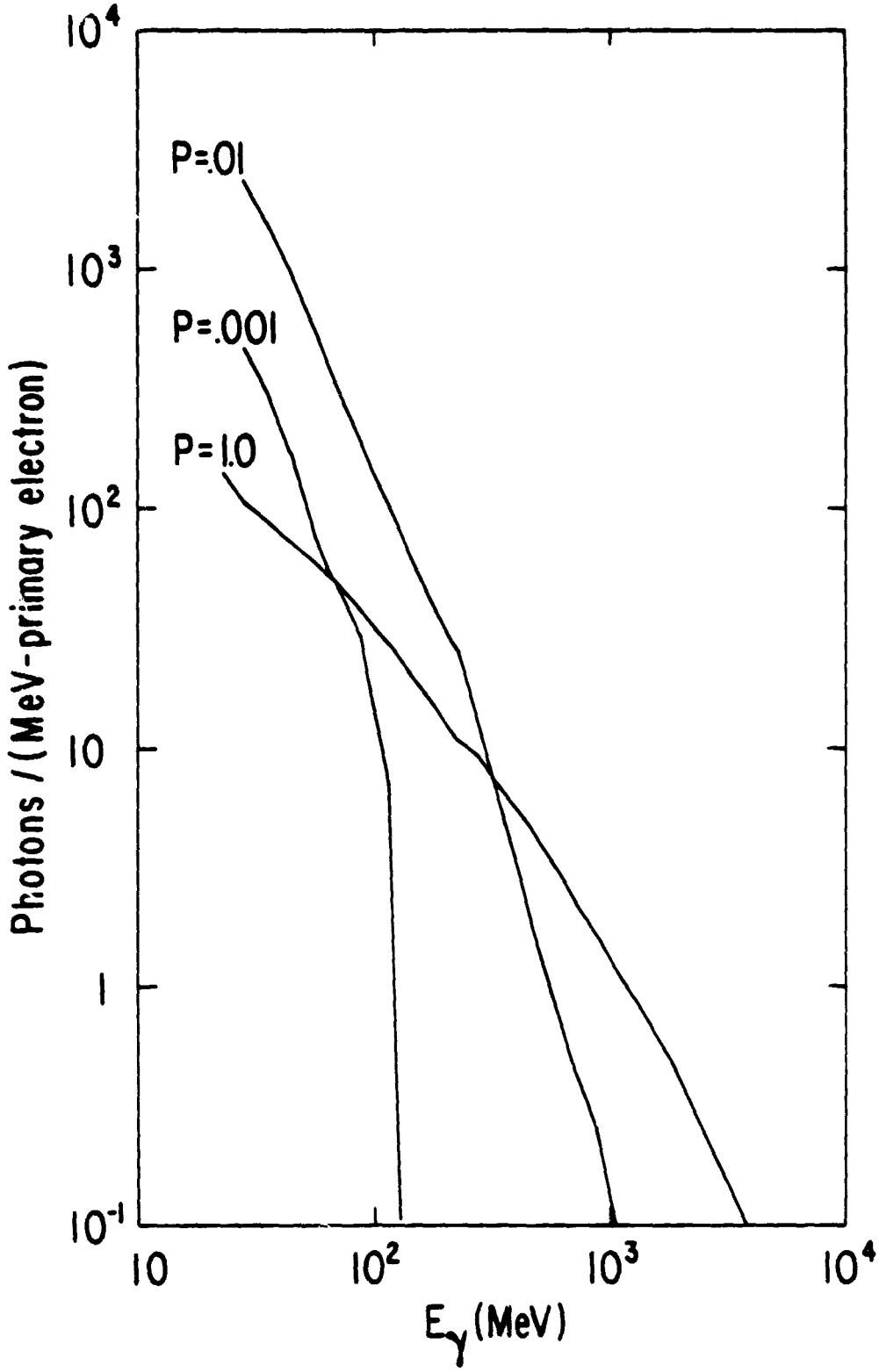
10^4
10^3
10^2
10
1
10^{-1}
P=.01
P=.001
P=1.0
Photons / (MeV-primary electron)
10
10^2
10^3
10^4
E_γ (MeV)

Figure 4

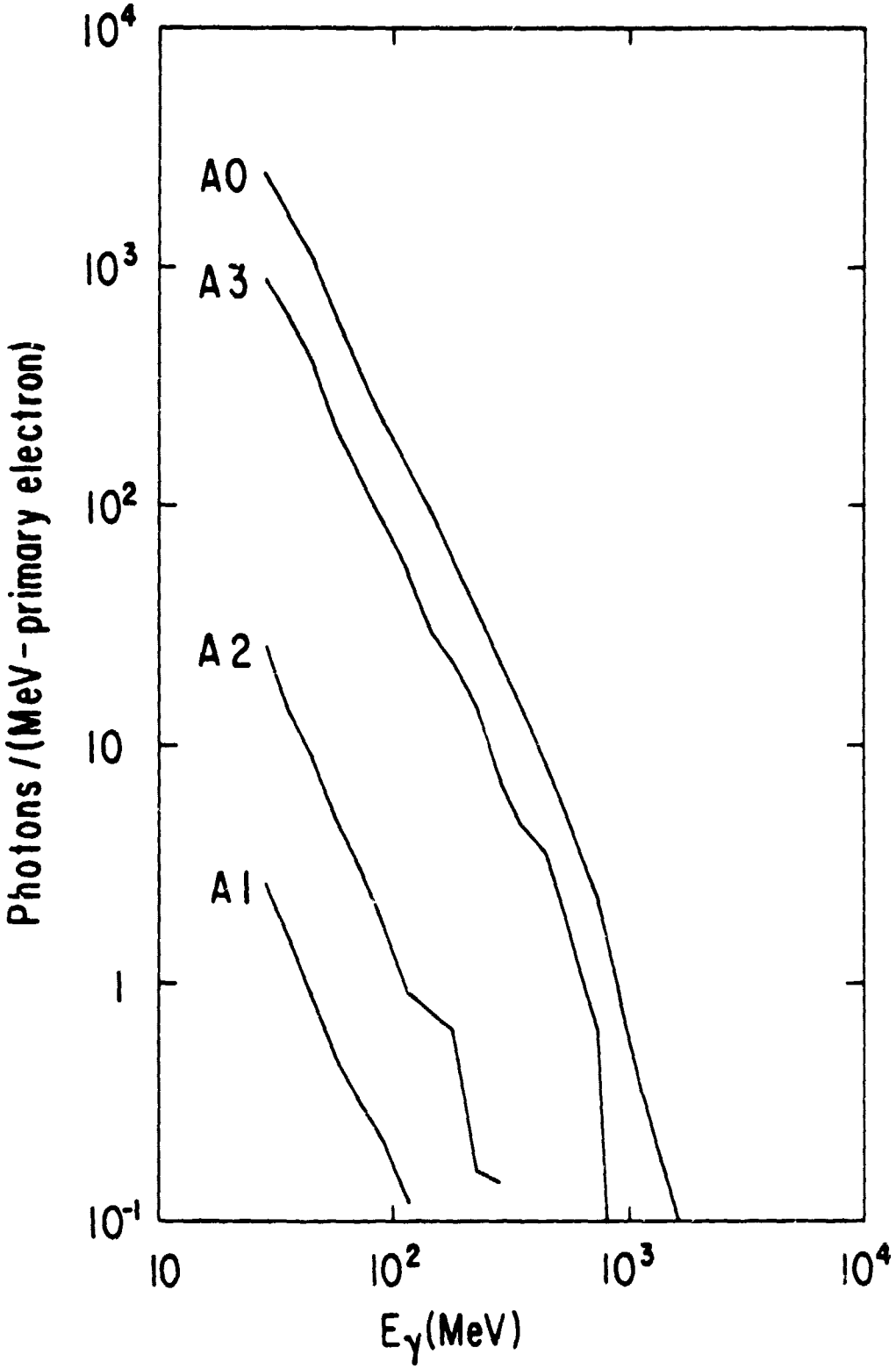
10^4
10^3
10^2
10
1
10^{-1}
A0
A3
A2
A1
Photons /(MeV-primary electron)
10
10^2
10^3
10^4
E_γ(MeV)

Figure 5

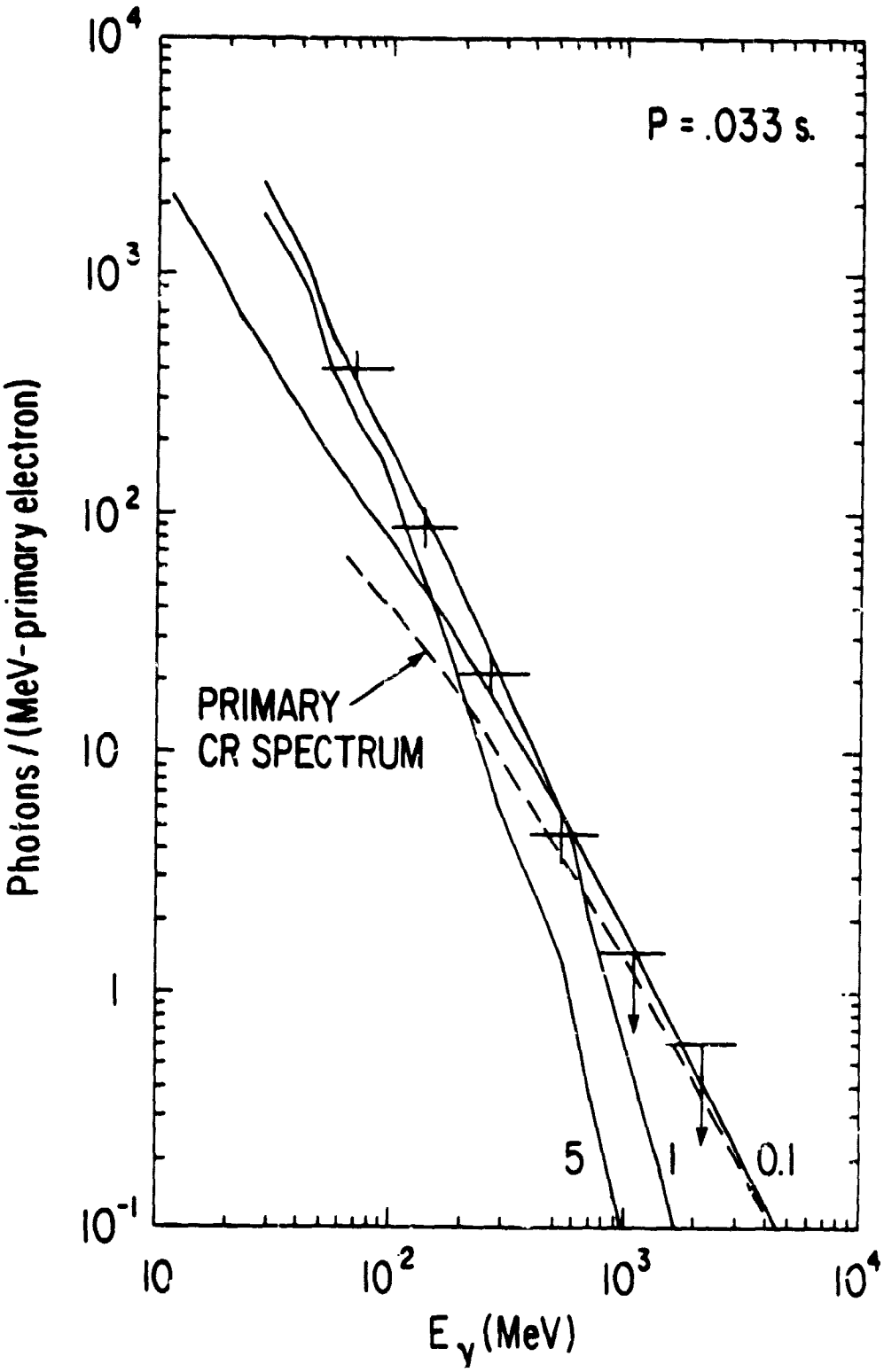
P = .033 s.
PRIMARY
CR SPECTRUM
5
1
0.1
Photons / (MeV-primary electron)
E_γ (MeV)
10^4
10^3
10^2
10
1
10^{-1}
10
10^2
10^3
10^4

Figure 6a

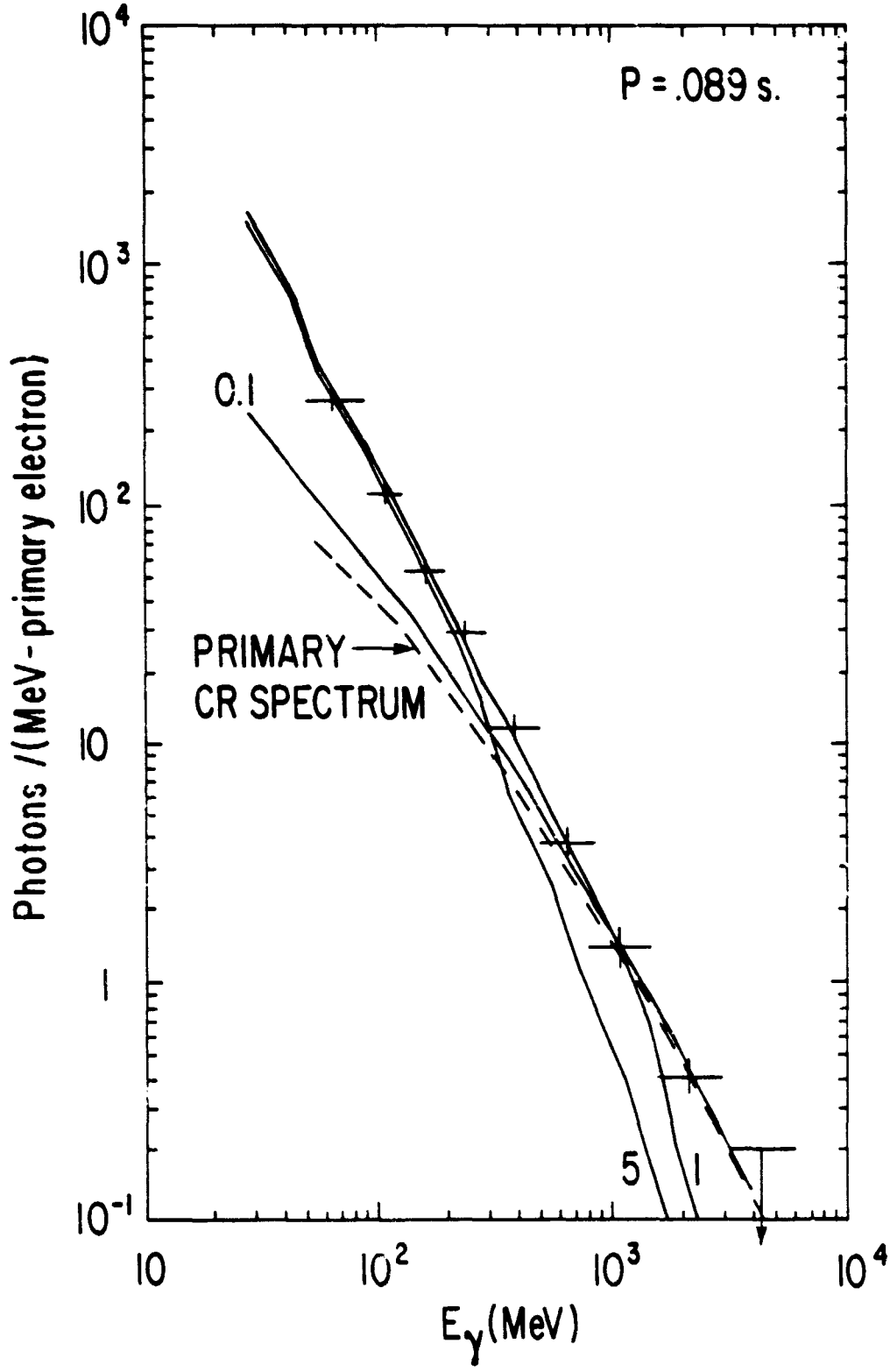
P = .089 s.
0.1
PRIMARY
CR SPECTRUM
5
1
Photons /(MeV-primary electron)
E_γ(MeV)
10^4
10^3
10^2
10
1
10^{-1}
10
10^2
10^3
10^4

Figure 6b

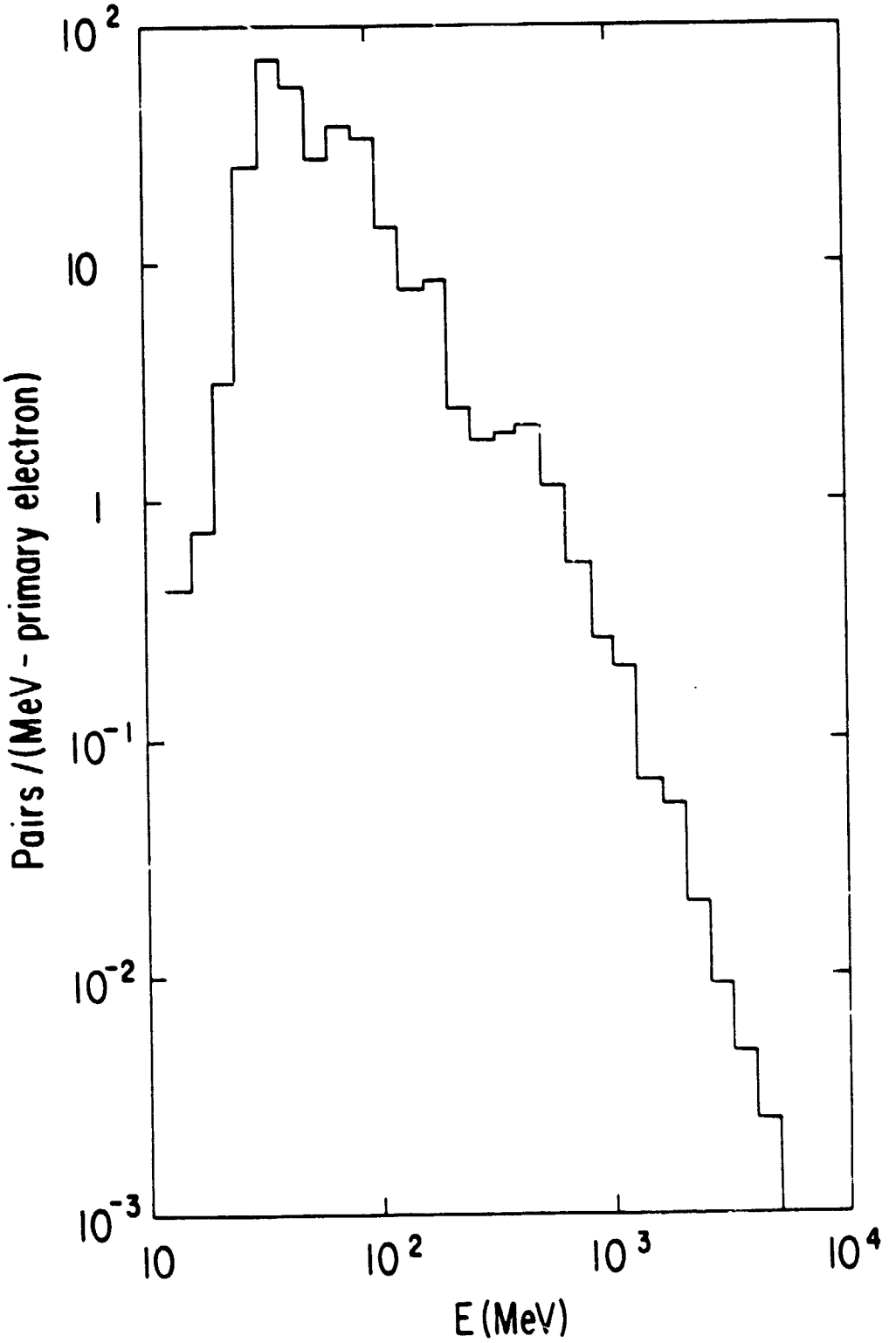
10^2
10
1
10^{-1}
10^{-2}
10^{-3}
Pairs /(MeV - primary electron)
10
10^2
10^3
10^4
E (MeV)

Figure 7

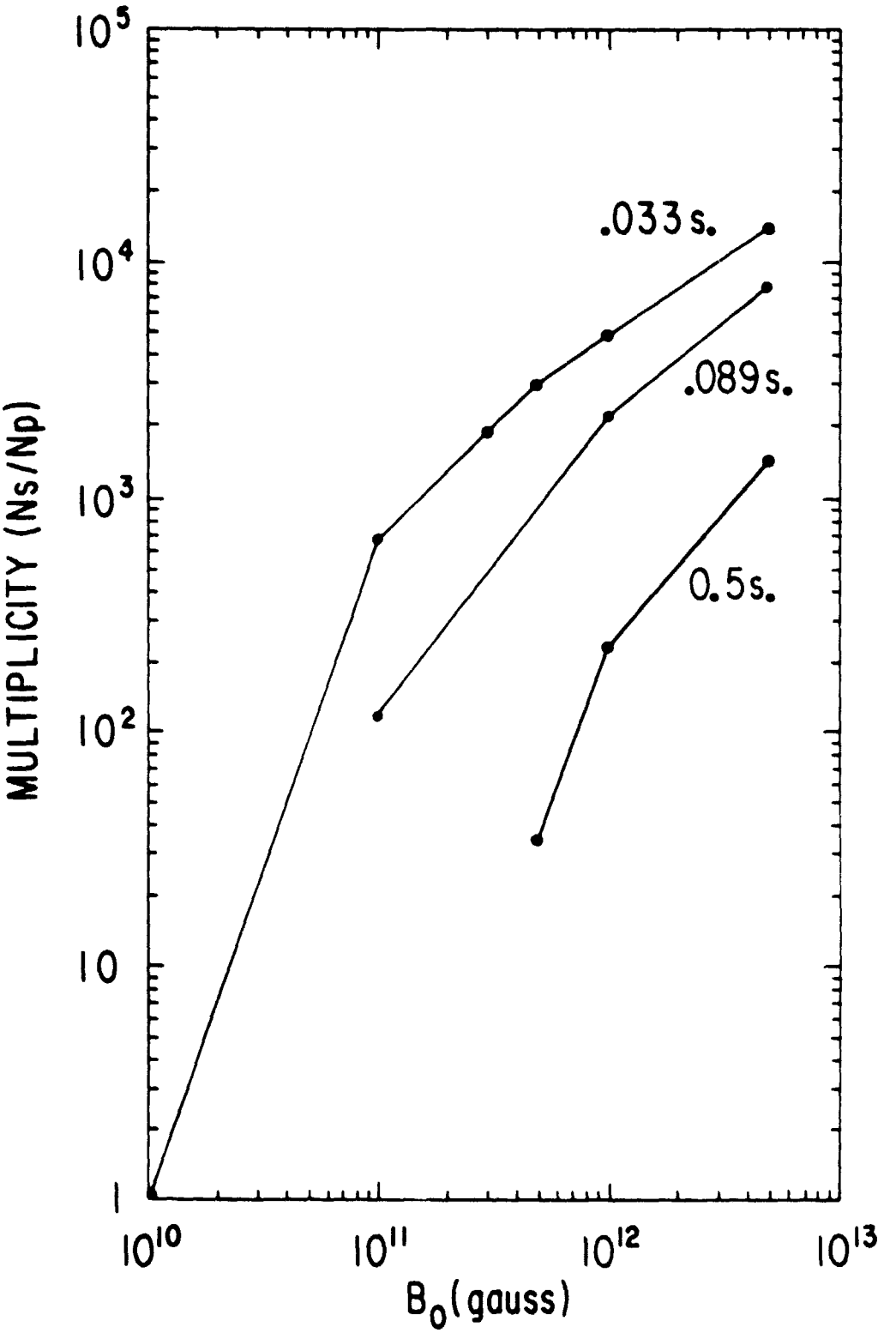
MULTIPLICITY (Ns/Np)
10^5
10^4
10^3
10^2
10
1
.033s.
.089s.
0.5s.
10^{10}
10^{11}
10^{12}
10^{13}
B_0(gauss)

Figure 8